

Comparative analysis of integrative and conjugative mobile genetic elements in the genus *Mesorhizobium*

Elena Colombi^{1,2,*}, Benjamin J. Perry³, John T. Sullivan³, Amanuel A. Bekuma^{4†}, Jason J. Terpolilli⁴, Clive W. Ronson³ and Joshua P. Ramsay^{1,2,*}

Abstract

Members of the *Mesorhizobium* genus are soil bacteria that often form nitrogen-fixing symbioses with legumes. Most characterised *Mesorhizobium* spp. genomes are ~8 Mb in size and harbour extensive pangenomes including large integrative and conjugative elements (ICEs) carrying genes required for symbiosis (ICESyms). Here, we document and compare the conjugative mobilome of 41 complete *Mesorhizobium* genomes. We delineated 56 ICEs and 24 integrative and mobilizable elements (IMEs) collectively occupying 16 distinct integration sites, along with 24 plasmids. We also demonstrated horizontal transfer of the largest (853,775 bp) documented ICE, the tripartite ICE_{MspSym}^{AA22}. The conjugation systems of all identified ICEs and several plasmids were related to those of the paradigm ICESym ICE_MSym^{R7A}, with each carrying conserved genes for conjugative pilus formation (*trb*), excision (*rdfS*), DNA transfer (*rlxS*) and regulation (*fseA*). ICESyms have likely evolved from a common ancestor, despite occupying a variety of distinct integration sites and specifying symbiosis with diverse legumes. We found extensive evidence for recombination between ICEs and particularly ICESyms, which all uniquely lack the conjugation entry-exclusion factor gene *trbK*. Frequent duplication, replacement and pseudogenization of genes for quorum-sensing-mediated activation and antiactivation of ICE transfer suggests ICE transfer regulation is constantly evolving. Pangenome-wide association analysis of the ICE identified genes potentially involved in symbiosis, rhizosphere colonisation and/or adaptation to distinct legume hosts. In summary, the *Mesorhizobium* genus has accumulated a large and dynamic pangenome that evolves through ongoing horizontal gene transfer of large conjugative elements related to ICE_MSym^{R7A}.

DATA SUMMARY

Bacterial genomes analysed in this study have been deposited previously in the National Centre for Biotechnology Information (NCBI) Genome database and are listed in Table S1 (available with the online version of this article). Genomes sequences produced in this study are deposited in NCBI, accession number NZ_NSFP00000000 and CP048406. Nine supplementary figures and seven supplementary tables are included in the online version of this article. Details on the

programmes and scripts used are available at <https://github.com/EC-Rufina/MesICE>.

INTRODUCTION

Horizontal gene transfer (HGT) is a major force shaping bacterial evolution [1–5]. Transfer of suites of genes encoding metabolic pathways refined by selection in a donor organism can endow recipients of HGT with the ability to colonise

Received 12 April 2021; Accepted 23 July 2021; Published 04 October 2021

Author affiliations: ¹Curtin Health Innovation Research Institute, Curtin University, Perth, WA, Australia; ²Curtin Medical School, Curtin University, Perth, WA, Australia; ³Department of Microbiology and Immunology, University of Otago, Dunedin, New Zealand; ⁴Centre for Rhizobium Studies, Food Futures Institute, Murdoch University, Perth, WA, Australia, Murdoch University, Perth, WA, Australia.

***Correspondence:** Elena Colombi, elena.colombi@curtin.edu.au; Joshua P. Ramsay, josh.ramsay@curtin.edu.au

Keywords: symbiosis; integrative and conjugative elements; ICE; IME; conjugation; mobilization; legumes; bacterial evolution; integrase; recombinase; tripartite ICE.

Abbreviations: ANI, average nucleotide identity; *att*, attachment; HGT, horizontal gene transfer; HMM, hidden Markov model; ICE, integrative and conjugative element; ICESym, symbiosis ICE; IME, integrative and mobilizable element; IS, insertion sequence; MGE, mobile genetic elements; *oriT*, origin of transfer; QS, quorum sensing; RDF, recombination directionality factor; T4CP, T4SS coupling-protein; T2SS, type II secretion system; T3SS, type III secretion system; T4SS, type IV secretion system.

†Present address: Western Australian Department of Primary Industries and Regional Development, Research and Industry Innovation, South Perth, WA, Australia.

Data statement: All supporting data, code and protocols have been provided within the article or through supplementary data files. Seven supplementary tables and nine supplementary figures are available with the online version of this article.

000657 © 2021 The Authors



This is an open-access article distributed under the terms of the Creative Commons Attribution License.

new ecological niches in a single evolutionary step [6–8]. Genome analyses suggest the most abundant type of conjugative elements in prokaryotes are integrative and conjugative elements (ICEs) [9]. ICEs are chromosomally-integrated elements that are passively replicated as a part of the genome but are capable of horizontal transmission facilitated by their encoded excision and conjugation systems [10, 11]. ICEs typically carry a conserved set of ‘backbone’ genes essential for ICE integration, excision, conjugation and regulation of transfer [12]. In addition to backbone genes, ICEs often carry accessory genes of adaptive significance to their hosts, such as genes affecting biofilm formation, pathogenicity, antibiotic and heavy metal resistance, bacteriocin synthesis, iron acquisition, and symbiosis [13–23]. During conjugative transfer, ICEs excise from the chromosome and circularise. ICE DNA is then nicked by a conjugative relaxase, and a single-stranded DNA copy of the ICE is transferred to the new host. Second strand synthesis, recircularization, and integration then occurs in donor and recipient cells [10, 11]. The conjugative machinery of ICEs and conjugative plasmids can also facilitate horizontal transfer of co-resident non-conjugative elements such as mobilizable plasmids and integrative mobilizable elements (IMEs) [24].

Gram-negative soil bacteria in the genus *Mesorhizobium* can establish a non-obligatory nitrogen-fixing symbiosis with legumes [25]. Symbiotic *Mesorhizobium* spp. infect legume root nodules, within which the bacteria fix atmospheric N₂ into NH₃, which is assimilated by the plant. In return the host plant supplies carbon, essential nutrients, and a niche for the microsymbiont. In *Mesorhizobium* spp., genes essential to the establishment of N₂-fixing associations are most often encoded on symbiosis ICEs (ICESyms) [19, 26–28] and occasionally on plasmids [29]. Symbiosis ICEs capable of horizontal transfer have been described in *Mesorhizobium* spp. isolated from nodules of *Lotus*, *Biserrula pelecinus* (*biserula*) and *Cicer* (chickpea) [19, 26–28, 30]. ICESyms have been observed to transfer to non-symbiotic mesorhizobia both in natural settings and laboratory conditions, converting them into symbionts [19, 26, 30].

ICEMISym^{R7A} was the first ICE described in *Mesorhizobium* spp. and it confers upon its host the ability to form N₂-fixing symbiosis with *Lotus* spp. [31]. The regulatory network controlling excision, conjugation and regulation of the ICE has been described in detail [32–36]. ICEMISym^{R7A} excision and integration is catalysed by the site-specific recombinase IntS. During integration of ICEMISym^{R7A} into the recipient chromosome, IntS catalyses recombination between a DNA site called *attP* on the circularised ICE and a corresponding *attB* site on the host chromosome, which for ICEMISym^{R7A} is the 3' end of the tRNA-Phe gene [19]. Integrase-mediated recombination between short identical ‘core’ sequences within *attP* and *attB* results in the integration of the ICE into the chromosome and the creation of two new attachment sites *attL* and *attR*, which flank the integrated ICE. Recently, ICESyms with a tripartite structure were described in *Mesorhizobium* spp. [26]. The tripartite ICE ICEMcSym¹²⁷¹ confers an ability to form a symbiosis with *Biserrula pelecinus*. ICEMcSym¹²⁷¹

Impact Statement

Nitrogen-fixing symbioses between legumes and rhizobia are a major contributor to global nitrogen cycling. For rhizobia of the genus *Mesorhizobium*, genes required for symbiosis are usually encoded on horizontally transmissible integrative and conjugative elements (ICEs). ICEs are important components of the bacterial accessory genome and key drivers of bacterial evolution but remain relatively unexplored compared with their plasmid counterparts. In this study, we performed a comparative analysis of mobile genetic elements identified in 41 complete *Mesorhizobium* genomes to gain insight into ICE distribution, evolution and structure. ICEs carrying symbiosis genes (ICESyms) likely evolved from a common ancestor and have subsequently diverged to integrate at a variety of chromosomal sites and specify symbiosis with several distinct legume hosts. Overall, the *Mesorhizobium* mobilome was dominated by ICEs and conjugative plasmids harbouring conjugation-gene clusters related to those of ICESyms and we observed extensive evidence of recombination between elements. Frequent rearrangement and duplication of genes controlling quorum sensing and ICESym transfer regulation suggested ICEs are undergoing extensive evolution to fine-tune their transferability. This study provides a significant advance in our understanding of *Mesorhizobium* genome organization and ICESym evolution.

and other tripartite ICEs possess three distinct site-specific integrases *intS*, *intM* and *intG*, that sequentially recombine three separate chromosomal regions α , β and γ , through three pairs of *attL* and *attR* sites, to form a single circular DNA element for conjugative transfer [37]. The tripartite α regions are the largest fragments of tripartite ICEs, and while the α regions lack integrase genes (which are encoded on fragments β and γ) they appear to carry most genes with known involvement in symbiosis and conjugative transfer.

The aim of this work was to characterise the mobilome of *Mesorhizobium* spp. in order to gain insight into its evolution. The accurate delineation of ICEs and large tripartite ICEs that frequently exceed 0.5 Mb in length requires complete and accurately assembled genomes. In this work, we interrogated 41 complete *Mesorhizobium* genome sequences and conducted a comparative analysis of conjugative and mobilizable elements. The *Mesorhizobium* spp. mobilome was found to be dominated by ICEs and conjugative plasmids with conjugation and regulatory genes related to ICEMISym^{R7A}. The various ICESyms specifying symbiosis with diverse legumes [26–28, 30] have likely evolved from a common ancestor within the larger family of proteobacterial ICEs [34, 38]. Extensive evidence for gene exchange between mobile elements suggests that ICEs, IME and plasmids have frequently recombined, swapped genetic cargo and their

mechanisms of host maintenance. Evidence of frequent rearrangement and duplications of quorum-sensing regulatory genes controlling the induction of ICESym mobilization suggest that the rates of ICE transfer are under continuing selection.

METHODS

Whole genome sequencing

Mesorhizobium sp. AA22 was sequenced both using Illumina HiSeq 2×100 bp paired-end reads (MrDNA) and the PacBio RSII platform (Macrogen, South Korea). PacBio raw reads were *de novo* assembled with Flye 2.6 [39]. The assembly was polished with the Pacbio reads five times using Minimap2 2.17-r941 [40] and Racon 1.4.3 [41]. The assembly was then further polished five times with the Illumina HiSeq reads using Pilon 1.23 [42]. The starting position of the genome was set with Circlator 1.5.5 [43].

The transconjugant strain *M. japonicum* R7ANSxAA22 was sequenced using Illumina MiSeq. Illumina sequence adapter contamination was removed using nesonclip (v0.132) (<https://github.com/Victorian-Bioinformatics-Consortium/nesoni>), and reads were corrected using Lighter (v1.1.1) [44] and assembled with SPAdes V. 3.5.0 [45].

Mesorhizobium genus phylogeny

The *Mesorhizobium* genus phylogeny was constructed using a method modified from Prokchorchik *et al.* [46]. Genomes (Table S1) were re-annotated using Prokka [47], and Proteinortho [48] was run with default settings to identify single-copy core genes. The nucleotide sequences of 1,609 single copy orthologues were then aligned with the MAFFT algorithm [49], and core gene alignments were concatenated and stripped of gaps with Goalign (<https://github.com/evolbioinfo/goalign>). Maximum likelihood phylogeny reconstruction was performed with RAxML v8.2.10 (parameters: -f a -p \$RANDOM -x \$RANDOM -N 100 m GTRCATX -T 16) [50]. The tree was rooted at midpoint using the midpoint() function from the phangorn package in R [51] and then it was visualised using FigTree v1.4.4 (<https://github.com/rambaut/figtree/>), only nodes with bootstrap values above 80 were displayed (Fig. S1).

Pairwise average nucleotide identity (ANI) was calculated using FastANI [52] on the entire genome of the strains. Strains were classified as same species if they showed an ANI of 95% or above [53].

Mobile genetic element search and pangenome classification

To identify putative horizontally transmissible elements, relaxase gene sequences were searched with hmmscan from HMMER [54] using available hidden Markov model (HMM) protein profiles (MOB database) [55] (Table S2) defined for distinct MOB-protein families [56]. For this search, a bit score threshold (-T) of 33 was used. For ambiguous classifications, the MOB-protein family was chosen by the best e-value in

the full sequence. For the identification of ICEs and IMEs, genomes were queried using the BLASTN algorithm [57] using *trbB* (EB234_29245) from ICESym^{R7A} [58], and *traA* (EB235_34495) from ICESym^{R88B} [59], here referred as IMEM^{R88b}. We used a cut off of 50% pairwise identity and, where applicable, only elements with recognisable *att* sites were selected (Table S3). Four pTONO-1-like sequences were present within chromosomal contig assemblies (CP034446.1, CP034447.1, CP034448.1, and CP034451.1). While it was possible that these plasmids were indeed chromosomally integrated, this seemed unlikely as each of the regions harboured plasmid-like replication genes (*repABC*), and *att* sites were not detected, suggesting the plasmid sequences were artificially joined to the chromosome sequence during assembly (Table S2).

The tool Phaster [60] was used to search all the genomes for potential prophage regions. Regions classified as 'intact' were inspected manually for the presence of capsid and tail proteins. Phage boundaries were delineated by the identification of direct sequence repeats (part of *att* core regions) produced following the integration of the phage in the genome (Table S3).

Core and accessory genome calculations were initially performed using iterative incrementation of the minimum percent identity threshold of BLASTP for the assignment in protein ortho-groups from 20–95% amino-acid identity (Fig. S2); to avoid underestimating the number of accessory gene orthologues, Proteinortho was run with default settings (25% identity) and reporting singleton genes.

Backbone identification

Backbone genes were identified as genes present in at least 95% of the elements, a threshold that was introduced to take into account sporadic deletion events. The identification of backbone genes was guided by Roary [61] and Proteinortho [48]. For Roary, a minimum amino-acid identity of 40% was used because with this cut-off the programme identified genes known to be involved in the ICE life cycle. Proteinortho was run with default settings. Both programmes identified the same set of conserved genes.

ICE comparative analysis

For all the following analyses, only non-redundant ICEs (Table S3) were used. Redundancy was defined based on overall gene content rather than by accumulation of SNPs, i.e. an element was considered redundant if it shared the same accessory genes as another ICE, with the exception of insertion sequences (IS). The nucleotide sequences of strictly conserved and single-copy backbone genes (Table S4) were aligned with the MAFFT algorithm [49], trimmed and concatenated in Geneious [62]. The alignment was used to build phylogeny of the elements using PhyML 3.3 [63] with 100 bootstrap replicates which was rooted at midpoint using the midpoint() function from the phangorn package in R [51]. This alignment was also used to build a neighbor-net tree with SplitTree [64], and to infer recombination with ClonalFrameML [65].

For the integrase and quorum sensing genes trees, nucleotide sequences were aligned with the MAFFT algorithm [49], the tree built with RAxML v8.2.10 (parameters as above) [50], and visualised with FigTree (v.1.4.4, <http://tree.bio.ed.ac.uk/software/figtree/>).

The *nod* box site motifs were identified as described in Perry et al. [28]. nhmmscan [66] was run using the training sets of previously characterised *nod* box sequences from ICEML-Sym^{R7A} and ICEMLSym^{NZP2037} [58, 67] as models.

Alfy [68] was used to identify chimaerism among ICEs and IMEs. Alfy was run selecting only matches with a *P* value <0.05 within a sliding window of 1000bp. Cytoscape [69] was then used to visualise the percentage of recombined sequences among ICEs, IMEs, and plasmids.

A distance matrix was calculated with the `dist.gene()` function from the `ape` package in R [70] using as input the gene presence-absence data produced by Roary run with a minimum amino-acid identity of 40%. The distance matrix was then used to build a neighbor-joining tree using the `nj()` function from the `ape` package in R [70]. eggNOG mapper 5.0 [71] was used for the functional annotation of accessory genes. Pangenome-wide association analyses of the ICEs were performed with Scoary [72]. *Mesorhizobium* sp. M1D.F.Ca. ET.043.01.1.1 harbours two ICESyms that carry redundant symbiosis genes and one of the two ICESyms (ICEMsp.Sym^{M1D-1}) appeared to be undergoing pseudogenization; for example it carried a truncated copy of *nodC* [27]. ICEMsp.Sym^{M1D-1} was therefore removed to avoid misleading the association analysis. To identify genes associated with symbiosis, Scoary was run on the output files produced by Roary that was run on all elements with minimum percentage identity for BLASTP of 40% and with paralogs not split. For the identification of genes associated with the host plant, Roary was run on only ICESyms using a minimum percentage identity for BLASTP of 70% and with paralogs not split. Full list of genes associated with symbiosis ICEs and associated with the host of isolation are reported in Tables S5 and S6 respectively.

Searches for antimicrobial resistance genes were performed using ResFinder v3.1 (<https://cge.cbs.dtu.dk/services/ResFinder/>), searches for bacteriocins and non-ribosomally synthesized and post-translationally modified peptides were performed with Bagel4 [73], and CRISPR-Cas systems with CRISPRDetect [74].

Conjugation experiments

M. japonicum R7ANS pFAJ1708-GFP [26] was used as recipient strain and *Mesorhizobium* sp. AA22 as donor strain. R7ANS is auxotrophic for biotin, nicotinate and thiamine, and the genes for the biosynthesis of biotin and nicotinate are present on ICEMsp.Sym^{AA22}, so exconjugants were selected on defined (G/RDM) medium containing thiamine (1 µg ml⁻¹) and tetracycline (2 µg ml⁻¹), but lacking biotin and nicotinate. Donor and the recipient were separately grown to stationary phase in liquid TY at 28 °C with shaking at 200 r.p.m. One millilitre of culture of donor and recipient

strains were pelleted by centrifugation at 14,000 r.p.m. for 1 min, resuspended together in 50 µl of TY, spotted onto TY agar plates, and incubated at 28 °C for 48 h. Spot matings were resuspended in sterile deionized water and serial dilutions were plated onto G/RDM supplemented with tetracycline and thiamine to select transconjugant strains, and onto G/RDM supplemented with thiamine to count donor strains. Plates were incubated at 28 °C for 7–10 days. The rate of conjugative transfer was calculated as the number of transconjugants per donor cell.

RESULTS AND DISCUSSION

Characterisation of complete *Mesorhizobium* genomes

Forty complete or nearly complete *Mesorhizobium* spp. genomes (Table S1) available from NCBI (updated April 2020) were analysed. The complete genome sequence of the *B. pelecinus* ssp. *pelecinus* symbiont *Mesorhizobium* sp. AA22 [75] was additionally completed in this study. A maximum-likelihood phylogeny inferred from a concatenated alignment of single-copy core genes revealed the 41 strains represented a genetically diverse group of mesorhizobia, and their ANI score showed they comprise 29 genospecies (Fig. S1). Most genomes analysed here are from strains isolated from root nodules of legume hosts *Cicer*, *Lotus* or *Biserrula* but also included are single strains isolated from *Astragalus sinicus* and *Robinia pseudoacacia*. Seven strains are from soil or aquatic environments.

Previous large-scale genome comparisons have revealed mesorhizobia harbour large and plastic pangenomes [27, 28]. Iterative pangenome analyses were carried out here with the 41 complete genomes using Proteinortho [48], initially using protein identity cut-offs ranging from 20–95% (Fig. S2). The estimated number of core genes remained largely unchanged with cut-off values between ~20–60%, but decreased above 60%, suggesting values <60% include most core genes without counting core genes from more distantly-related species as distinct orthologues. Using a 25% cut-off, the average genome in this dataset encoded 6386 proteins of which 1670 (26%) were part of the core genome.

Identification of ICEs, IMEs, conjugative plasmids and mobilizable plasmids in complete *Mesorhizobium* genome sequences

Conjugative DNA relaxases - also referred to as 'Mob' proteins - are DNA endonucleases that target and nick the origin-of-transfer sequences present on mobile genetic elements. Relaxases are required for recruitment of ssDNA of conjugative and mobilizable elements to the conjugative type IV secretion system (T4SS) for transfer. Relaxase proteins have been assigned into six MOB families: MOB_P, MOB_H, MOB_Q, MOB_C, MOB_P and MOB_V [76]. MOB_P is the largest family and includes the TraI relaxase of the broad-host range plasmid RP4; the MOB_F family includes the TraI relaxase of the F plasmid, and MOB_Q, which partially overlaps with the MOB_P family, includes various tumour-inducing (Ti) plasmids of

ICE regions in the chromosome. In total, 56 ICEs across 38 genomes were delineated (Table S3). The *att* sites were not identified for four ICEs (Table S2). Delineated ICEs ranged in length from 65,889 bp for ICEM^{NZP2042}, to 853,775 bp for the tripartite ICE, ICEM^{AA22}. All ICEs identified carried ICEM^{R7A}-related conjugation-gene clusters. Genes for nitrogen fixation and symbiosis were identified on 34 ICEs and these are hereafter collectively referred to as ICESyms. Thirteen of the ICESyms were tripartite in structure and carried the same three pairs of *att* sites and integrase genes as the paradigm tripartite ICE ICEM¹²⁷¹. Monopartite ICESyms of *Mesorhizobium* spp. isolated from *Lotus* were all integrated adjacent to the tRNA-Phe gene, while monopartite *Cicer* ICESyms were integrated adjacent to a tRNA-Ser gene (Table S3) as documented for *M. ciceri* CC1192 [30]. ICEs lacking symbiosis genes were identified adjacent to tRNA-Met, tRNA-Arg, tRNA-Gly, tRNA-His, and tRNA-Pro genes, as well as *guaA*, *radC* and *dusA*. Chromosomal boundaries for 24 putative MOB_F-carrying IMEs (Table S3) were delineated. IMEs ranged in size from 5,814 bp (IMEM^{M2A.E05-1}) to 271,605 bp (IMEM^{NZP2077-1}). Three IMEs were integrated adjacent to a tRNA-Asn gene, while the remaining 21 utilised the same spectrum of *att* sites as ICEs (*radC*, tRNA-Met, tRNA-Arg, tRNA-Phe and tRNA-Ser genes). IMEM^{M2A.E02-2} (40,024 bp) and the MOB_Q-carrying IME, IMEM^{W5M1284} (98,929 bp), occupied unique sites adjacent to tRNA-Thr and tRNA-Trp genes, respectively. In total, the 79 identified ICEs and IMEs collectively occupied 16 distinct integration sites within the 41 *Mesorhizobium* genomes (Table S7). Seventy-three of the elements carried integrase genes encoding tyrosine recombinases and serine recombinases/integrases were present on five IMEs and one ICE.

Five of the 13 conjugative plasmids identified carried conjugation-gene clusters related to that of ICEM^{R7A} and the remaining eight carried conjugation-gene clusters resembling the *vir*-like T4SS system of pTONO-1 (Fig. 1). Conjugative plasmids with ICESym-like T4SS genes ranged in size from 208,315 bp (pMLb of MAFF303099) to 648,231 bp (pMc1192 of CC1192) and none of these carried a complete set of nodulation or nitrogen-fixation genes. pMc1192 was recently shown to be not essential for N₂ fixation with chickpea [30]. Overall, most genomes contained at least one ICE (1.22±0.85 ICE per genome) and less frequently IMEs (0.5±0.7 IME per genome). Twenty-five genomes contained no plasmids, nine contained a single plasmid and seven harboured multiple plasmids. *M. oceanicum* sp. B7, *M. sp. 8*, *M. amorphae* CCNWGS0123 and *M. sp. 7653R* were the only strains lacking any detectable ICEs or IMEs and, interestingly, CCNWGS0123 and 7653R were also the only strains carrying a complete complement of genes required for nodulation and nitrogen fixation on plasmids. Only the symbiosis plasmid of CCNWGS0123 carried a conjugation-gene cluster (*vir*-like).

The identified mobile genetic elements (MGE) carry approximately 12% the identified pangenome. This suggests a major fraction of the pangenome is either located on unidentified MGE or that most of the pangenome genes have lost mobility and now form a large but stable fraction of each chromosome.

For the pangenome genes identified on MGEs, i.e. the mobile pangenome or mobilome, ~72% were present on ICEs and of these, 78% were present on ICESyms (Fig. S3). Plasmids and IMEs carried 20.4 and 5.9% of the mobilome, respectively, while bacteriophages carried only 4.6%.

ICES in *Mesorhizobium* share a conserved core-gene organisation

Proteinortho [48] and Roary [61] were used to identify protein-coding genes conserved across 95% of ICEs and plasmids carrying an ICEM^{R7A}-like conjugation-gene cluster. Both tools identified 17 backbone genes including the ICEM^{R7A} conjugation-gene cluster (T4SS) genes *msi031*, *trbBCDEJLFGI* and *msi021*, the T4CP gene *traG*, the relaxase *rlxS*, the putative peptidoglycan transglycosylase gene *msi107*, the *traF* prepilin peptidase gene and the RDF gene *rdfS*. Genes encoding the DUF736 domain (*msi110* on ICEM^{R7A}) were present on all elements (Fig. S4), often in duplicate. Concatenated DNA alignments of the single-copy backbone genes (Table S4) were used to generate a maximum likelihood tree (Fig. 2a). Despite the association of ICESyms with a variety of integrase genes and chromosomal integration sites, the tree grouped all monopartite and tripartite ICESyms into a single clade that exhibited lower average sequence divergence (88% pairwise nucleotide identity) than other ICEs (69% pairwise nucleotide identity). Only one ICE lacking symbiosis genes (ICEM^{M2A.E046}) grouped with the ICESyms. ICESyms present in strains isolated from the same plant genus grouped together (with the exception of ICEM^{AA22}), even though alignments used to produce the tree only included genes with transfer-related functions. Interestingly, all identified ICESyms (and ICEM^{M2A.E046}) lack the conjugation entry exclusion gene *trbK* [58, 81], genes encoding a putative Rep_3 superfamily replication initiator, and DUF2840-domain protein located between *rdfS* and *traF* (Figs 1 and S4), which were present on all other ICEs identified. These genes are present on distantly related ICEs and plasmids found throughout the proteobacteria, including Tn4371 [34, 38], suggesting gene loss occurred in a common ancestor of the ICESyms. Conjugative plasmids pMLb and pCC1192 clustered closely with ICEs present in separate branches of the tree, suggesting the conjugation-gene clusters on these elements may have switched between ICE and plasmid modes of host maintenance. All plasmids carrying an ICEM^{R7A}-like conjugation system retained the *rdfS* gene, which in ICEM^{R7A} and ICEM¹²⁷¹ stimulates integrase-mediated ICE excision [32, 37]. RdfS is also a transcriptional regulator [36, 37], so it may have additional regulatory roles in transfer, which may explain its retention on plasmids [9].

Comparisons of ICE backbone gene phylogeny and ICE integration site suggested there was no strict association between the two. The phylogenies of tripartite ICE integrase genes (Fig. S5) and their ICE backbone genes (Fig. 2a) were also incongruent. While the tripartite ICEs carry closely related IntG and IntM integrases that group separately from similar integrase genes on monopartite ICEs, the transfer genes of

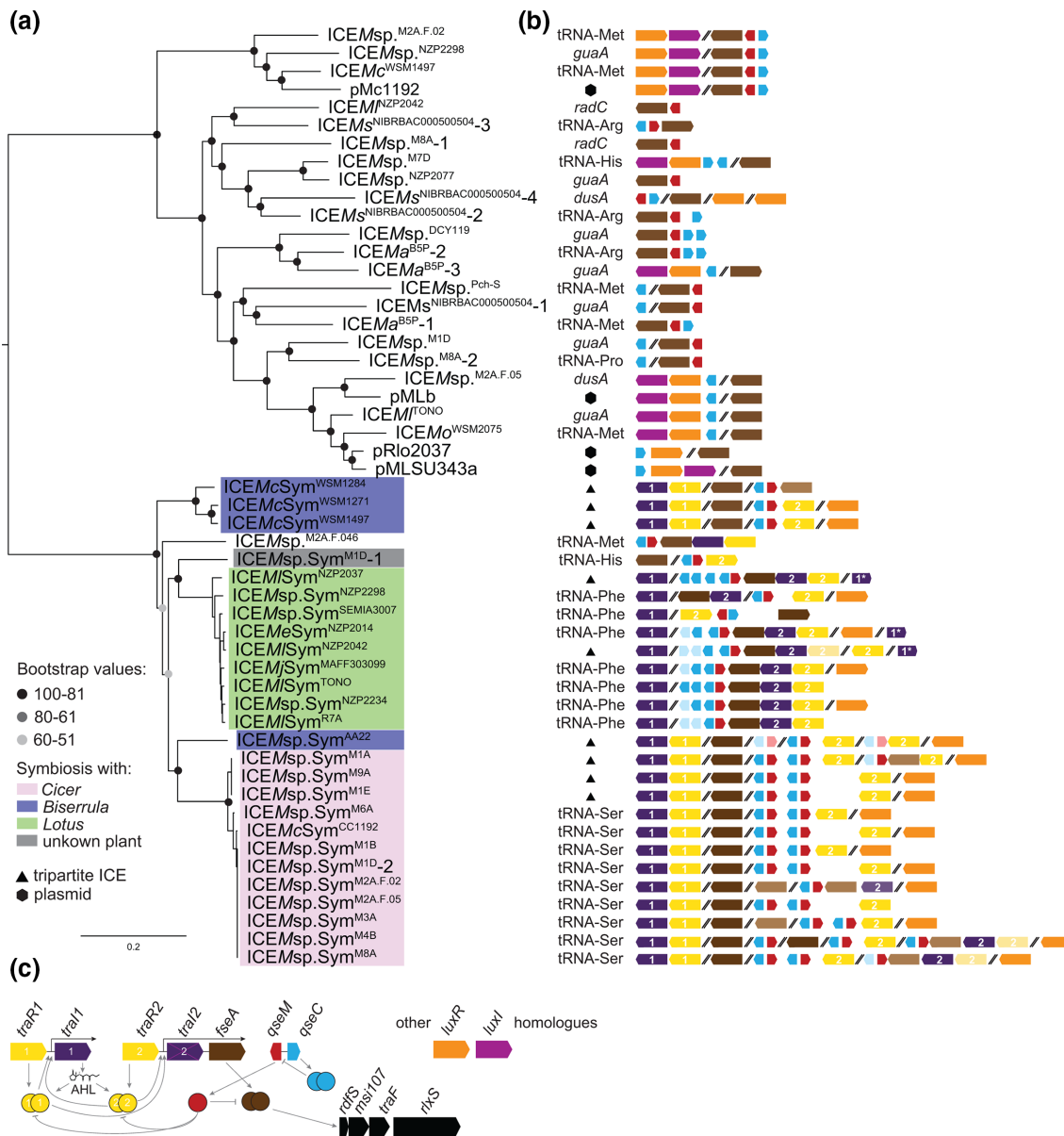


Fig. 2. ICE phylogeny and regulatory-gene organisation. (a) PhyML tree based on the concatenation of alignments of 15 single-copy backbone genes, scale bar indicates substitutions per site. (b) Organization of regulatory genes colour-coded as in c, lighter boxes are likely pseudogenes, numbers in *traR* and *traI* indicate the relatedness between the copies as described in main text, * indicates the gene is truncated. (c) Regulatory network activating ICE transfer in ICEMSym^{R7A} and ICEMcSym¹²⁷¹.

monopartite and tripartite ICEs present in *Lotus*-associated mesorhizobia are more closely related to each other than they are to those of tripartite ICEs present in *Cicer*-associated mesorhizobia and vice versa.

Gene duplications and pseudogenization have shaped quorum sensing and transfer regulation on ICESyms

Excision and conjugative transfer of ICEMSym^{R7A} and the tripartite ICE, ICEMcSym¹²⁷¹, are activated by quorum sensing; however, they carry different arrangements of *traR*

and *traI* genes. ICEMSym^{R7A} carries a single copy of the QS regulator gene *traR* (or *msi174*, referred to here as *traR2*) and two acyl-homoserine lactone synthase genes named *traI1* and *traI2*. While the TraI2 sequence shares 65% amino-acid identity with TraI1, the *traI2* gene is not essential for AHL production and an in-frame deletion of *traI2* is not affected for ICEMSym^{R7A} excision or transfer [33]. Conversely, ICEMcSym¹²⁷¹ lacks *traI2* altogether, but carries two functional copies of *traR* (*traR1* and *traR2*) encoding proteins with 54% amino-acid identity, and a single copy of *traI* (*traI1*). Here we searched for TraR/TraI homologues

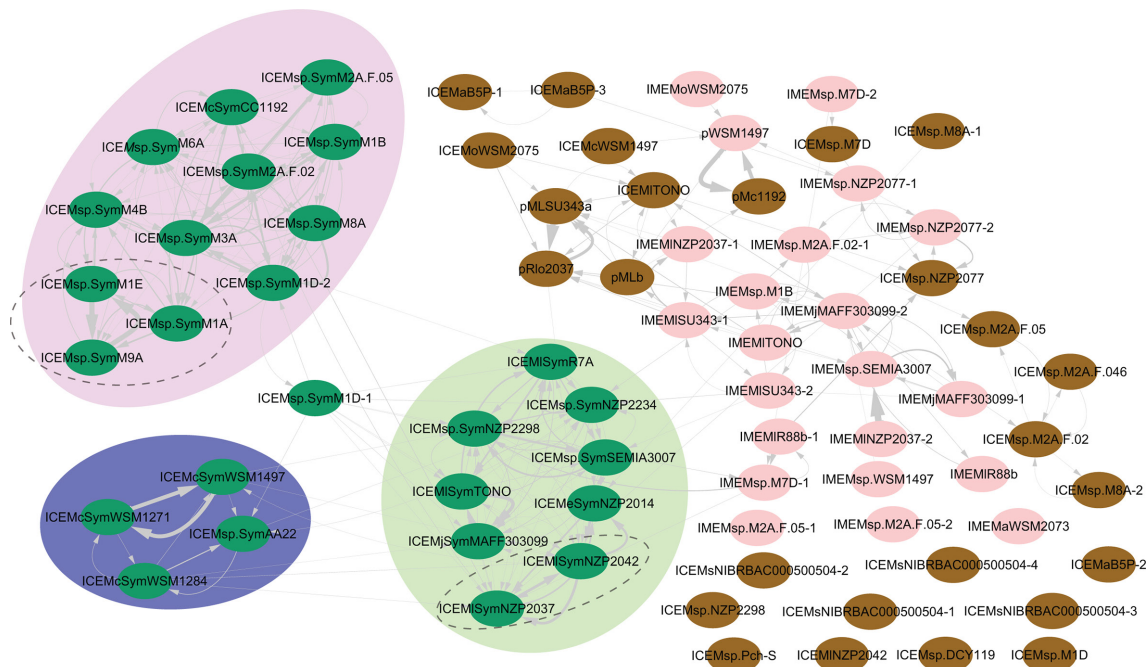


Fig. 3. Recombination detected between and among ICEs, IMEs and plasmids. Cytoscape network produced with recombination analysis between ICE, IME and plasmid genes. Elements associated with brown circles are ICEs and plasmids lacking symbiosis genes, ICESyms are green while IMEs and the mobilizable plasmid pWSM1497 are pink. The coloured regions indicate highlight ICESyms associated with *Biserrula* (blue), *Lotus* (green) and *Cicer* (lilac). The tripartite ICEs are circled with a dashed line. Arrows between elements start from the query sequence used in Alfy nine and point to the element within which homologous regions were detected. Arrow width is proportional to the additive length of the sequences exhibiting homology.

encoded on ICESyms, which revealed further variations in copy number and gene organisation of the *traR* and *traI* genes (Figs 2b and S6). While additional genes encoding TraR/LuxR-family regulators were also identified both on ICESyms and other ICEs and plasmids, the predicted proteins were distantly related (~25% amino-acid identity). All but one ICESyms and ICEMsp.^{M2A.F.046} carried *traI1* but mostly only *Lotus*-associated ICESyms carried a copy of *traI2*. No *Lotus*-associated ICESyms carried a copy of *traR1*, but closer inspection revealed that a ~100 bp remnant of the 3' end of *traR1* was present directly upstream of each *traI1*, confirming that an ancestral copy of *traR1* had been deleted in this ICE lineage. Nucleotide alignments of the eight *traI2* and eight *traI1* genes on *Lotus*-ICESyms revealed that *traI2* sequences collectively carried 147 unique SNPs, 92 amino-acid changes and two frame-shifting deletions. In contrast, *traI1* genes exhibited lower divergence with only 23 unique SNPs (13 synonymous). This suggests the *traI2* alleles, while conserved on *Lotus*-associated ICESyms, are at various stages of pseudogenization. These observations support our previous proposal [37] that gene duplication of the *traR-traI* locus occurred in an ancestor of the ICESym clade and subsequently different ICESyms have variably lost one of the duplicates.

On ICEMISym^{R7A}, both TraR2 and the activator of *rdjS* expression, FseA, are inhibited by the antiactivator QseM [35]. *qseM* expression is controlled by an adjacently-encoded

helix-turn-helix protein QseC (Fig. 2c). Searches for *qseM* and *qseC* genes on ICEs revealed numerous duplications and rearrangements. ICESyms of *Lotus* and *Biserrula* each harboured one copy of *qseM* and multiple variants of *qseC*. In some instances, *qseC* variants carried mutations and/or deletions likely rendering them non-functional (Fig. 2b). All *Cicer* lineage ICEs harboured at least two distinct copies of paired *qseM-qseC* genes, with the exception of ICEMsp.Sym^{M2A.F.02}. The presence of two copies of *qseM* in the *Cicer*-associated ICESyms suggests that there may be distinct inputs controlling each *qseM* gene, or perhaps the two QseM proteins may target the two TraR proteins also encoded by these ICEs with differing affinities. In summary, both positive and negative regulators controlling QS and conjugative transfer have been frequently duplicated, pseudogenized and rearranged on ICESyms, suggesting that natural selection is constantly adjusting the regulation of ICESym transfer.

Cargo genes of conjugative and mobilizable elements

Functional annotation by eggNOG mapper [71] of the accessory genes on ICESyms indicated 56% had putative metabolic roles. Of these, 27% were likely involved in amino-acid metabolism and transport, 24% in energy production, and 16% in coenzyme metabolism. Similarly, a major portion of the accessory genes (43%) carried by other ICEs and

related plasmids were predicted to be involved in metabolism, including 28% potentially involved in amino-acid metabolism and transport, and 25% in energy production and conversion. Collectively ICESyms carried 11,726 genes, with 2,200 (19%) genes present on one ICE only. Only 66 accessory genes were present on all ICESyms, while no accessory genes were universally conserved ICES lacking symbiosis genes, which collectively encoded 4,037 genes, of which 1,830 were present on one ICE only (45%). A similar pattern was observed for IMEs, which collectively carried 3,195 accessory genes, 47% of which were encoded by one IME only. No antibiotic-resistance genes, bacteriocins, non-ribosomally synthesized or post-translationally modified peptides were detected on any of the ICES and IMEs (ResFinder v3.1, Bagel4 [73]). ICES_{NIBRBAC000500504}-2 carried putative resistance-genes for arsenic, cadmium, and mercury, while ICES_{NIBRBAC000500504}-3 carried putative resistance-genes for mercury and chromate.

While the above analyses suggested that all ICES and plasmids carry a highly variable spectrum of genetic cargo, a neighbor-joining tree based solely on the presence/absence of ICE accessory genes (Fig. S7) clearly separated ICESyms from other ICES and plasmids, and also separated ICESyms based on their host-strain legume association. Comparative analysis of ICESym gene cargo with that of other ICES identified genes specific to ICESyms (Table S5). As expected, these included genes coding for the synthesis and maturation of active nitrogenase (*nif* genes), for a bacteroid electron transfer flavoprotein complex and for a low O₂ *cbh*₃-type cytochrome oxidase (*fix* genes), genes participating in the biosynthesis and secretion of Nod factors (*nodABC* and *nodIJ*) and the recognition of plant flavonoids (*nodD2*). *fixV*, the key upstream regulator of the *nif* genes in R7A [67], was also present on all ICESyms. Conserved genes uninvestigated for roles in *Lotus*, *Cicer* and *Biserrula* symbiosis were also identified. A putative inosose isomerase with similarity to *Sinorhizobium meliloti* pSymB protein SMb20711 [82] was present in all ICESyms encoded adjacent to *nodD2*. Genes required for production of the queuosine precursor PreQ₀, *queCDE*, were present on all ICESyms but not on other ICES. Queuosine is a modified guanosine nucleotide base present on some tRNAs. In *S. meliloti*, *queC* appears to be required for an effective symbiosis with *Medicago trunculata* [83]. All *Lotus*-associated ICESyms also carry a second PreQ₀ synthesis cluster with genes ordered *queEDC*. All ICESyms carried at least one copy of *dctA*, coding for a C₄-dicarboxylate transport protein essential for nitrogen fixation [84]. In the *Lotus* lineage ICES, a single copy of *dctA* was paired with cognate regulatory genes *dctBD*, while in the other ICESyms only *dctA* was present. The *Cicer*-associated ICES and ICESym^{A22} harboured two copies of *dctA*. In *S. meliloti* pSymB, the expression of *dctA* is dependent on *dctBD* in free-living conditions but during symbiosis, *dctA* is efficiently expressed even in the absence of *dctBD* [85].

An association analysis was carried out comparing ICESym genes based on the host of isolation to identify genes that might be of specific adaptive significance for each host (Table S6). ICESym genes specifically associated with *Cicer*-associated mesorhizobia included the type III secretion

system (T3SS) effector gene *nopP* and two hypothetical genes. These two hypothetical protein-coding genes are likely to code for T3SS effectors as they are preceded by T3SS boxes [86] and they were predicted to be secreted (SecP score >0.73) by SecretomeP [87]. In *Bradyrhizobium* spp., variations in *nopP* alleles control soybean host compatibility [88]. All *Cicer*-associated ICESyms carry the nodulation gene *nodH* and a type II secretion system (T2SS) gene cluster. Using nhmmscan [66] and a hidden Markov model profile generated from characterised *nod* box sequences [28], we identified a putative *nod*-box motif upstream of the T2SS gene cluster in CC1192 (CP0150621 coordinates: 4,306,615–4,306,661). Although the potential role of T2SS in symbiosis is not known, numerous phytopathogens employ T2SS systems for secretion of plant-tissue degrading enzymes [89]. It is possible that ICESym T2SS systems have a role in root colonization or infection. The ICESyms of *Lotus*-isolated mesorhizobia uniquely carry nodulation genes *nodS* (*msi131*), *noeJ* (*msi383*) and *noeK* (*msi384*), and an uncharacterised operon (*msi322* to *msi327*, and previously not-annotated EB234_30895 between *msi323* and *msi324*) encoding putative aspartate and asparagine metabolism-related enzymes. No ICESym genes were significantly associated with strains specifically isolated from *Biserrula* hosts (Bonferroni $P < 0.05$).

Gene flux between MGEs

ICES can exchange genes with other MGEs through several mechanisms, including IS-mediated transposition and inter-ICE/IME/plasmid recombination [23, 90–92]. To detect evidence for inter-ICE recombination we used the neighbor-net algorithm [93] to create a network representing the relationship between the backbone genes present on ICES and plasmids (Fig. S8). Patterns of reticulation within the network supported inter-ICE recombination even between highly conserved and contiguous ICE backbone genes (Phi test for recombination [94] was $P < 0.0001$). Analyses with ClonalFrameML [65] also indicated recombination events between backbone genes. The alignment-free programme Alfy was used to extend the analysis to include entire gene content of ICES, IMEs, and plasmids sequences [68]. Extensive evidence of gene exchange between ICES and IMEs was detected. Clustering of ICES based on evidence for gene exchange separated ICESyms from other ICES and IMEs, suggesting greater gene exchange between ICESyms and little recombination between ICESyms and other ICES or IMEs (Fig. 3). When this analysis was repeated using only contiguous gene clusters present on all ICESyms (Fig. S9), most of the connections indicative of DNA exchange between ICESyms reduced from 172 to 79, suggesting a large proportion of the detected recombination events represent homologous recombination between conserved ICESym regions.

Given the extensive inter-ICESym recombination detected in the previous analyses, we interrogated some of the sequences in more detail. A comparison of the QS loci of the *Lotus* associated ICESyms ICESym^{MAFF303099}, ICESym^{NZP2037} and ICESym^{R7A}, revealed several disruptions in average nucleotide identity between the three regions (Fig. 4a). In

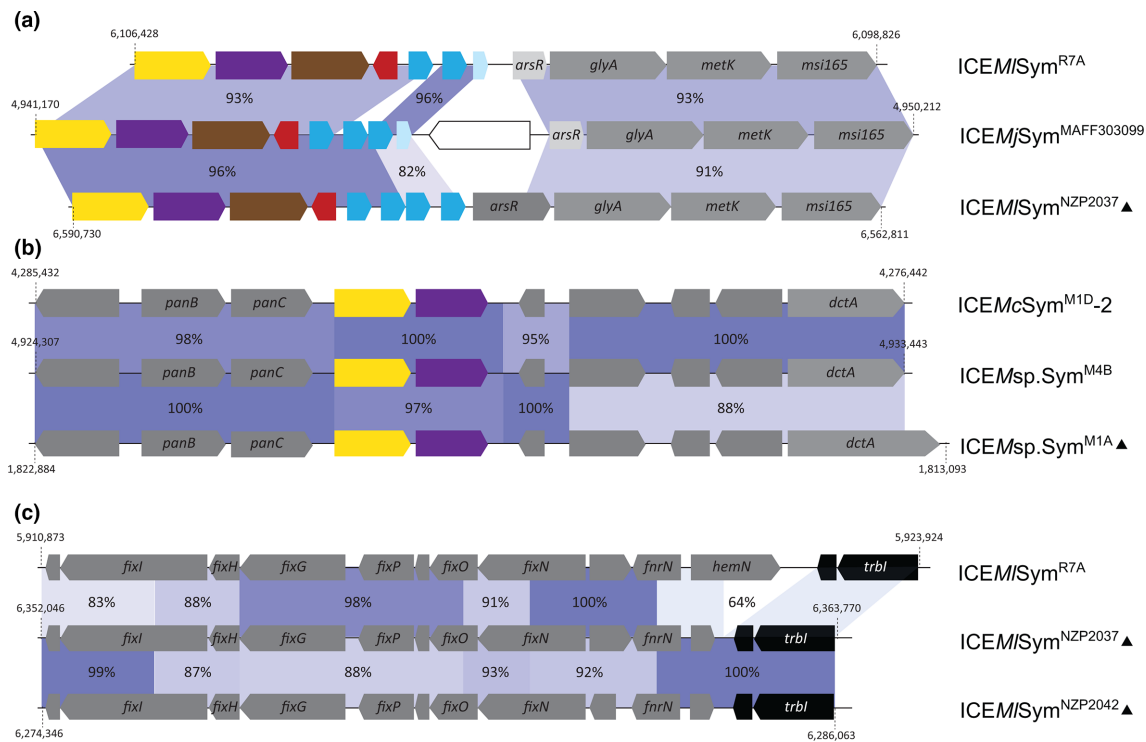


Fig. 4. Chimaeric ICESym loci. Genes coding for QseC proteins are coloured in azure, *qseM* is displayed in red, *fseA* in brown, *traI* in purple, *traR* in yellow, and insertion sequences in white. Black indicates backbone genes, other genes are shown in grey, light-grey boxes indicate pseudogenes. Blue-shaded areas between genes on different ICESyms indicate homologous regions and the pairwise nucleotide identity is indicated. The triangle indicates tripartite ICE. (a) Comparison of the quorum-sensing-gene loci on ICEMjSym^{MAFF303099}, ICEMISym^{NZP2037} and ICEMISym^{R7A}. (b) Comparison of the quorum-sensing-gene loci on ICEMcSym^{M1D-2}, ICEMsp.Sym^{M4B} and ICEMsp.Sym^{M1A}. (c) Comparison of the *fix*-gene loci on ICEMISym^{NZP2037}, ICEMISym^{NZP2042} and ICEMISym^{R7A}.

ICEMjSym^{MAFF303099}, the nucleotide sequence between *traR2* and the second copy of *qseC* was 96% identical to tripartite ICEMISym^{NZP2037}, however, downstream of the copy of *qseC* the nucleotide identity reduced to 82% but shared 96% identity to a region on ICEMISym^{R7A}. The QS locus in ICEMsp.Sym^{M4B} appeared to be a chimaera of the ICEMcSym^{M1D-2} and tripartite ICEMsp.Sym^{M1A}, carrying alternating regions of 100% pairwise nucleotide identity shared with these two ICEs (Fig. 4b). We also identified clear evidence for ancestral recombination between the *fix*-gene loci of ICEMISym^{NZP2037}, ICEMISym^{NZP2042} and ICEMISym^{R7A} (Fig. 4c).

The largest documented horizontally mobile ICE, ICEMspSym^{AA22}

Mesorhizobium sp. AA22 was isolated from *Biserrula pelecinus* and carries a tripartite ICE with a total length of 853,775 bp, making ICEMspSym^{AA22} the largest ICE identified in any bacterium to date. The α , β and γ fragments are 766,834, 70,134 and 16,815 bp in length respectively. The other tripartite ICEs have α , β and γ fragments sized between 443,551 and 563,069 bp, between 19,361 and 74,018 bp, and between 5,412 bp and 25,603 bp respectively, indicating that most of the expansion in ICEMspSym^{AA22} size has occurred within the α fragment. To determine if ICEMspSym^{AA22} was mobile, we carried out conjugation experiments using the ICE-cured *M. japonicum*

R7A derivative R7ANS as a recipient [32]. ICEMspSym^{AA22} transferred with an average frequency of 6.0×10^{-8} exconjugants per donor (standard deviation 2.3×10^{-8}). An exconjugant was isolated and sequenced using short-read sequencing. *De novo* assembly (NZ_NSNFP00000000) confirmed each of the *attL* and *attR* site junctions were present and mapping of the exconjugant reads to the AA22 sequence confirmed the entire ICEMspSym^{AA22} had transferred and recombined with the R7ANS chromosome as expected [26].

Pangenome analysis highlighted several gene clusters unique to ICEMspSym^{AA22}. For instance, ICEMspSym^{AA22} harbours a complete *nuo* (NADH:ubiquinone oxidoreductase) gene cluster located at the beginning of the α fragment. The ICEMspSym^{AA22} *nuo* cluster is distinct from that coded for on the AA22 chromosome both in gene order and nucleotide identity (maximum identity observed of 59.6% for *nuoM*). Interestingly, the ICEMspSym^{AA22} *nuo* cluster shares the same gene arrangement and 81.7% average pairwise nucleotide identity to that encoded on the symbiosis plasmid pSymA of *S. meliloti* [95].

ICEMspSym^{AA22} is also the only ICE in *Mesorhizobium* to carry a CRISPR-Cas system. The type I-C CRISPR-Cas system (CP048406.1, coordinates: 6,182,785–6,192,544) harbours *cas3*, *cas5*, *cas8* and *cas7*; however it lacks *cas4*, *cas1* and *cas2*

involved in spacer acquisition [96, 97]. The CRISPR locus harbours over 40 spacers interspersed with non-identical palindromic repeats. The targets of the spacers (identified via BLASTN and CRISPRTarget [98]) appear similar to putative phage and plasmid sequences, some of which are found in other soil bacteria such as *Mesorhizobium*, *Rhizobium*, *Streptomyces*, *Azospirillum*, *Agrobacterium* and *Paraburkholderia*.

CONCLUSIONS

In this work we analysed 41 complete *Mesorhizobium* spp. genomes to enumerate the conjugative and mobilizable elements present. Of the pangenome genes present on an identifiable MGE (12%), more than 70% were present across 56 ICEs related to ICEMISym^{R7A}, including the largest mobile ICE characterised to date, ICEMsp.Sym^{A22}. The remaining mobilome spanned 24 plasmids, 27 IMEs and 17 bacteriophages. On average, each genome carried at least one ICE (1.22±0.85) and 50% of strains carried an IME. In contrast, of the 41 genomes examined, only 16 carried plasmids and only seven genomes harboured multiple plasmids.

The ICESyms formed a clear monophyletic group distinct from the other identified mesorhizobial ICEs. Presumably, following the capture of symbiosis genes by an archetypal ICESym, descendants diverged into ICESyms that specify symbiosis with different legumes. It is unclear if this archetypal ICESym evolved within the *Mesorhizobium* genus or was acquired from outside the genus. It is also unclear why symbiosis plasmids, which are the most common form of symbiosis MGE in other rhizobia, are rarely identified in *Mesorhizobium* spp. In *Rhizobium* spp. symbiosis plasmids predominantly carry *vir*-like conjugation systems [99] and interestingly, the only conjugative mesorhizobial symbiosis plasmid identified in this analysis (in CCNWGS0123) also carries a *vir*-like conjugation system. Thus there seems to be no intrinsic barrier to establishment of these conjugative symbiosis plasmids in *Mesorhizobium*. Broader genomic comparisons suggest ICEs generally have a larger host range than their plasmid counterparts [100], so it may be that once established in *Mesorhizobium* spp., ICESyms have been more successful infiltrating diverse members of the genus. Regardless of the mechanistic or evolutionary reasons, it is clear from these analyses that ICEs dominate the mobilome of nitrogen-fixing legume symbionts of the *Mesorhizobium* genus.

The ICEs and IMEs identified in this work were found integrated within 16 distinct sites in the chromosome and carried an overlapping set of integrase genes and integration sites. The phylogeny of ICE backbone genes suggests some ICEs have switched between integration sites during evolution and some ICEs even appear to have become plasmids in several branches of the tree (e.g. pMLb and pCC1192). Overall these observations mirror those made from broader analyses of ICEs, IME and plasmids in bacteria [100]. Given the ubiquity of conjugative elements identified in these genomes, we suspect that the frequent switching of integration mechanisms by these elements reflects fierce competition for chromosomal integration sites amongst ICEs and IME in this genus.

There is clear evidence that some ICESyms have likely switched from a monopartite to a tripartite structure. The tripartite-ICE integrase genes specifying integration at tRNA-Met(a) and *guaA* are distinct from their closest counterparts on monopartite ICEs (Fig. S5) suggesting the tripartite ICE recombination system evolved once. The observation that the tripartite ICEs structure appears at multiple positions in the ICE backbone tree suggests that tripartite ICEs have likely recombined with monopartite ICESyms and replaced the recombination systems on these ICEs.

We identified numerous instances of gene duplications, pseudogenization, rearrangements and recombination between loci involved in quorum sensing (*traR* and *traI*) and its inhibition (*qseM* and *qseC*) (Figs 2 and 4). In contrast, the gene organisation of conjugation-gene clusters and *rdfS*, *traF* and *rlxS* genes remained remarkably conserved even between very distantly related plasmids and ICEs. The frequent rearrangements of top-level regulators of transfer may reflect the conflicting evolutionary forces faced by ICEs, which must balance their evolutionary trajectories between vertical and horizontal descent. High frequency ICE transfer may increase the likelihood that an ICE will arrive in a new host with superior attributes but high transfer rates could also tax the bacterial host resources and hence be subject to negative selection. Dysregulation of quorum sensing resulting from two ICESyms in the same cell might also drive the observed rearrangements. Consistent with this possibility, introduction of an extra copy of *traR* and the preceding promoter region on a low-copy plasmid is enough to activate AHL production, ICEMISym^{R7A} excision and conjugative transfer in *M. japonicum* R7A [32, 33]. Interestingly, in the only strains in this dataset carrying two ICESyms (*Mesorhizobium* sp. M1D.F.Ca.ET.043.01.1.1 and M2A.F.Ca.ET.046.03.2.1) one of these ICESyms, ICEMsp.Sym^{M1D}-1, is also the only ICESym lacking a copy of the *traI* AHL-synthase gene (Fig. 2b).

Our analysis of gene flux between MGE suggests a substantial amount of homologous recombination occurs between the ICESyms and in particular, ICESyms specifying symbiosis with the same legume host. There are several explanations why recombination may occur more readily between the ICESyms than other ICEs. More closely related ICESyms are more likely to utilise the same integration sites and therefore integrate in tandem in the same locus, a situation known to promote ICE recombination [90]. The frequency of homologous recombination is exponentially more likely to occur between the closely-related sequences of the ICESyms (88% backbone pairwise nucleotide identity) than with less related ICEs (69% backbone pairwise nucleotide identity) [101]. Mesorhizobia that participate in symbiosis with the same legume host may occupy the same niche, providing greater opportunity for ICESyms to encounter each other in the same cell through HGT. An interesting observation from the comparisons of conserved ICE backbone genes is that all ICESym and ICEMsp.^{M2A.F.046} lack the *trbK*, tentatively indicating ICESyms have lost one mechanism to inhibit entry of competing ICESyms. This

could suggest that homologous recombination has been an integral part of ICESym evolution and that loss of *trbK* has contributed by increasing the opportunity for two ICESyms to meet in the same cell.

Funding information

J.P.R., is the recipient of an Australian Research Council Future Fellowship (Project ID FT170100235) funded by the Australian Government. This work was supported by Australia Awards Africa for AAB.

Author contributions

Conceptualization: E.C., J.P.R. Funding: J.P.R. Methodology: E.C., J.P.R. Formal analysis: E.C., J.P.R. Investigation: E.C., J.P.R., A.B., J.J.T., B.J.P. Visualization: E.C. Writing – original draft preparation: E.C., J.P.R. Writing – review and editing: E.C., J.P.R., B.J.P., J.T.S., A.B., J.J.T., C.W.R. Supervision: J.P.R., C.W.R.

Conflicts of interest

The authors declare that there are no conflicts of interest.

References

- Mirkin BG, Fenner TI, Galperin MY, Koonin EV. Algorithms for computing parsimonious evolutionary scenarios for genome evolution, the last universal common ancestor and dominance of horizontal gene transfer in the evolution of prokaryotes. *BMC Evol Biol* 2003;3:2.
- Kunin V, Goldovsky L, Darzentas N, Ouzounis CA. The net of life: Reconstructing the microbial phylogenetic network. *Genome Res* 2005;15:954–959.
- Dagan T, Martin W. Ancestral genome sizes specify the minimum rate of lateral gene transfer during prokaryote evolution. *Proc Natl Acad Sci U S A* 2007;104:870–875.
- Halary S, Leigh JW, Cheaib B, Lopez P, Baptiste E. Network analyses structure genetic diversity in independent genetic worlds. *Proc Natl Acad Sci U S A* 2010;107:127–132.
- Kloesges T, Popa O, Martin W, Dagan T. Networks of gene sharing among 329 proteobacterial genomes reveal differences in lateral gene transfer frequency at different phylogenetic depths. *Mol Biol Evol* 2011;28:1057–1074.
- Caro-Quintero A, Konstantinidis KT. Inter-phylum HGT has shaped the metabolism of many mesophilic and anaerobic bacteria. *ISME J* 2015;9:958–967.
- Fondi M, Karkman A, Tamminen MV, Bosi E, Virta M, et al. “Every gene is everywhere but the environment selects”: global geolocalization of gene sharing in environmental samples through network analysis. *Genome Biol Evol* 2016;8:1388–1400.
- Lawrence JG. Gene transfer in bacteria: Speciation without species? *Theor Popul Biol* 2002;61:449–460.
- Guglielmini J, Quintais L, Garcillán-Barcia MP, de la Cruz F, Rocha EPC. The repertoire of ice in prokaryotes underscores the unity, diversity, and ubiquity of conjugation. *PLoS Genet* 2011;7:e1002222.
- Wozniak RAF, Waldor MK. Integrative and conjugative elements: Mosaic mobile genetic elements enabling dynamic lateral gene flow. *Nat Rev Microbiol* 2010;8:552–563.
- Johnson CM, Grossman AD. Integrative and conjugative elements (ices): What they do and how they work. *Annu Rev Genet* 2015;49:577–601.
- Delavat F, Miyazaki R, Carraro N, Pradervand N, van der Meer JR. The hidden life of integrative and conjugative elements. *FEMS Microbiol Rev* 2017;41:512–537.
- Peters SE, Hobman JL, Strike P, Ritchie DA. Novel mercury resistance determinants carried by INCJ plasmids PMERPH and r391. *Mol Gen Genet* 1991;228:294–299.
- Rauch PJ, De Vos WM. Characterization of the novel nisin-sucrose conjugative transposon Tn5276 and its insertion in *Lactococcus lactis*. *J Bacteriol* 1992;174:1280–1287.
- Ravatt R, Studer S, Springael D, Zehnder AJ, van der Meer JR. Chromosomal integration, tandem amplification, and deamplification in *Pseudomonas putida* F1 of a 105-kilobase genetic element containing the chlorocatechol degradative genes from *Pseudomonas* sp. Strain B13. *J Bacteriol* 1998;180:4360–4369.
- Beaber JW, Hochhut B, Waldor MK. Genomic and functional analyses of SXT, an integrating antibiotic resistance gene transfer element derived from *Vibrio cholerae*. *J Bacteriol* 2002;184:4259–4269.
- Drenkard E, Ausubel FM. *Pseudomonas* biofilm formation and antibiotic resistance are linked to phenotypic variation. *Nature* 2002;416:740–743.
- Burrus V, Marrero J, Waldor MK. The current ICE age: Biology and evolution of sxt-related integrative and conjugative elements. *Plasmid* 2006;55:173–183.
- Sullivan JT, Ronson CW. Evolution of rhizobia by acquisition of a 500-kb symbiosis island that integrates into a *phe*-tRNA gene. *Proc Natl Acad Sci U S A* 1998;95:5145–5149.
- Dimopoulou ID, Kartali SI, Harding RM, Peto TEA, Crook DW. Diversity of antibiotic resistance integrative and conjugative elements among haemophili. *J Med Microbiol* 2007;56:838–846.
- Heather Z, Holden MTG, Steward KF, Parkhill J, Song L, et al. A novel streptococcal integrative conjugative element involved in iron acquisition. *Mol Microbiol* 2008;70:1274–1292.
- Kung VL, Ozer EA, Hauser AR. The accessory genome of *Pseudomonas aeruginosa*. *Microbiol Mol Biol Rev* 2010;74:621–641.
- Colombi E, Straub C, Künzel S, Templeton MD, McCann HC, et al. Evolution of copper resistance in the kiwifruit pathogen *Pseudomonas syringae* pv. *actinidiae* through acquisition of integrative conjugative elements and plasmids. *Environ Microbiol* 2017;19:819–832.
- Guédon G, Libante V, Coluzzi C, Payot S, Leblond-Bourget N. The obscure world of integrative and mobilizable elements, highly widespread elements that pirate bacterial conjugative systems. *Genes (Basel)* 2017;8:337.
- Laranjo M, Alexandre A, Oliveira S. Legume growth-promoting rhizobia: an overview on the *Mesorhizobium* genus. *Microbiol Res* 2014;169:2–17.
- Haskett TL, Terpolilli JJ, Bekuma A, O’Hara GW, Sullivan JT, et al. Assembly and transfer of tripartite integrative and conjugative genetic elements. *Proc Natl Acad Sci U S A* 2016;113:12268–12273.
- Greenlon A, Chang PL, Damte ZM, Muleta A, Carrasquilla-Garcia N, et al. Global-level population genomics reveals differential effects of geography and phylogeny on horizontal gene transfer in soil bacteria. *Proc Natl Acad Sci U S A* 2019;116:15200–15209.
- Perry BJ, Sullivan JT, Colombi E, Murphy RJT, Ramsay JP, et al. Symbiosis islands of lotaeae-nodulating *Mesorhizobium* comprise three radiating lineages with concordant *nod* gene complements and nodulation host-range groupings. *Microb Genom* 2020;6.
- Wang X, Luo Y, Liu D, Wang J, Wei S, et al. Complete genome sequence of the *Robinia pseudoacacia* L. symbiont *Mesorhizobium amorphae* CCNWGS0123. *Stand in Genomic Sci* 2018;13:18.
- Hill Y, Colombi E, Bonello E, Haskett T, Ramsay J, et al. Evolution of diverse effective N₂-fixing microsymbionts of *Cicer arietinum* following horizontal transfer of the *Mesorhizobium ciceri* CC1192 symbiosis integrative and conjugative element. *Appl Environ Microbiol* 2020.
- Sullivan JT, Patrick HN, Lowther WL, Scott DB, Ronson CW. Nodulating strains of rhizobium loti arise through chromosomal symbiotic gene transfer in the environment. *Proc Natl Acad Sci U S A* 1995;92:8985–8989.
- Ramsay JP, Sullivan JT, Stuart GS, Lamont IL, Ronson CW. Excision and transfer of the *Mesorhizobium loti* R7A symbiosis island requires an integrase INTS, a novel recombination directionality factor RDFS, and a putative relaxase RLXS. *Mol Microbiol* 2006;62:723–734.
- Ramsay JP, Sullivan JT, Jambari N, Otori CA, Heeb S, et al. A LuxRI-family regulatory system controls excision and transfer of

- the *Mesorhizobium loti* strain R7A symbiosis island by activating expression of two conserved hypothetical genes. *Mol Microbiol* 2009;73:1141–1155.
34. Ramsay JP, Major AS, Komarovskiy VM, Sullivan JT, Dy RL, et al. A widely conserved molecular switch controls quorum sensing and symbiosis island transfer in *Mesorhizobium loti* through expression of a novel antiactivator. *Mol Microbiol* 2013;87:1–13.
 35. Ramsay JP, Tester LGL, Major AS, Sullivan JT, Edgar CD, et al. Ribosomal frameshifting and dual-target antiactivation restrict quorum-sensing-activated transfer of a mobile genetic element. *Proc Natl Acad Sci U S A* 2015;112:4104–4109.
 36. Verdonk CJ, Sullivan JT, Williman KM, Nicholson L, Bastholm TR, et al. Delineation of the integrase-attachment and origin-of-transfer regions of the symbiosis island ICEMISymR7A. *Plasmid* 2019;104:102416.
 37. Haskett TL, Terpolilli JJ, Ramachandran VK, Verdonk CJ, Poole PS, et al. Sequential induction of three recombination directionality factors directs assembly of tripartite integrative and conjugative elements. *PLoS Genet* 2018;14:e1007292.
 38. Toussaint A, Merlin C, Monchy S, Benotmane MA, Leplae R, et al. The biphenyl- and 4-chlorobiphenyl-catabolic transposon Tn4371, a member of a new family of genomic islands related to IncP and Ti plasmids. *Appl Environ Microbiol* 2003;69:4837–4845.
 39. Kolmogorov M, Yuan J, Lin Y, Pevzner PA. Assembly of long, error-prone reads using repeat graphs. *Nat Biotechnol* 2019;37:540–546.
 40. Li H. Minimap2: Pairwise alignment for nucleotide sequences. *Bioinformatics* 2018;34:3094–3100.
 41. Vaser R, Sović I, Nagarajan N, Šikić M. Fast and accurate *de novo* genome assembly from long uncorrected reads. *Genome Res* 2017;27:737–746.
 42. Walker BJ, Abeel T, Shea T, Priest M, Abouelliel A, et al. Pilon: An integrated tool for comprehensive microbial variant detection and genome assembly improvement. *PLoS One* 2014;9:e112963.
 43. Hunt M, Silva ND, Otto TD, Parkhill J, Keane JA, et al. Circlator: Automated circularization of genome assemblies using long sequencing reads. *Genome Biol* 2015;16:294.
 44. Song L, Florea L, Langmead B. Lighter: fast and memory-efficient sequencing error correction without counting. *Genome Biol* 2014;15:509.
 45. Bankevich A, Nurk S, Antipov D, Gurevich AA, Dvorkin M, et al. Spades: A new genome assembly algorithm and its applications to single-cell sequencing. *J Comput Biol* 2012;19:455–477.
 46. Prokhorchik M, Pandey A, Moon H, Kim W, Jeon H, et al. Host adaptation and microbial competition drive *Ralstonia solanacearum* phylotype I evolution in the Republic of Korea. *Microb Genom* 2020;6:e000461.
 47. Seemann T. PROKKA: Rapid prokaryotic genome annotation. *Bioinformatics* 2014;30:2068–2069.
 48. Lechner M, Findeiss S, Steiner L, Marz M, Stadler PF, et al. Proteinortho: detection of (co-)orthologs in large-scale analysis. *BMC Bioinformatics* 2011;12:124.
 49. Katoh K, Standley DM. MAFFT multiple sequence alignment software version 7: Improvements in performance and usability. *Mol Biol Evol* 2013;30:772–780.
 50. Stamatakis A. RAxML version 8: A tool for phylogenetic analysis and post-analysis of large phylogenies. *Bioinformatics* 2014;30:1312–1313.
 51. Schliep KP. PHANGORN: Phylogenetic analysis in R. *Bioinformatics* 2011;27:592–593.
 52. Jain C, Rodriguez-R LM, Phillippy AM, Konstantinidis KT, Aluru S. High throughput ANI analysis of 90k prokaryotic genomes reveals clear species boundaries. *Nat Commun* 2018;9:1–8.
 53. de Lajudie PM, Andrews M, Ardley J, Eardly B, Jumas-Bilak E, et al. Minimal standards for the description of new genera and species of rhizobia and agrobacteria. *Int J Syst Evol Microbiol* 2019;69:1852–1863.
 54. Eddy SR. Accelerated profile HMM searches. *PLoS Comp Biol* 2011;7:10.
 55. Abby SS, Cury J, Guglielmini J, Néron B, Touchon M, et al. Identification of protein secretion systems in bacterial genomes. *Sci Rep* 2016;6:1–14.
 56. Francia MV, Varsaki A, Garcillán-Barcia MP, Latorre A, Drains C, et al. A classification scheme for mobilization regions of bacterial plasmids. *FEMS Microbiol Rev* 2004;28:79–100.
 57. Altschul SF, Gish W, Miller W, Myers EW, Lipman DJ. Basic local Alignment Search Tool. *J Mol Biol* 1990;215:403–410.
 58. Sullivan JT, Trzebiatowski JR, Cruickshank RW, Gouzy J, Brown SD, et al. Comparative sequence analysis of the symbiosis island of *Mesorhizobium loti* strain R7A. *J Bacteriol* 2002;184:3086–3095.
 59. Reeve W, Sullivan J, Ronson C, Tian R, Bräu L, et al. Genome sequence of the *Lotus corniculatus* microsymbiont *Mesorhizobium loti* strain R88B. *Stand in Genomic Sci* 2014;9:3.
 60. Arndt D, Grant JR, Marcu A, Sajed T, Pon A, et al. PHASTER: A better, faster version of the PHAST phage search tool. *Nucleic Acids Res* 2016;44:W16–21.
 61. Page AJ, Cummins CA, Hunt M, Wong VK, Reuter S, et al. Roary: Rapid large-scale prokaryote pan genome analysis. *Bioinformatics* 2015;31:3691–3693.
 62. Kearse M, Moir R, Wilson A, Stones-Havas S, Cheung M, et al. Geneious basic: An integrated and extendable desktop software platform for the organization and analysis of sequence data. *Bioinformatics* 2012;28:1647–1649.
 63. Guindon S, Dufayard J-F, Lefort V, Anisimova M, Hordijk W, et al. New algorithms and methods to estimate maximum-likelihood phylogenies: Assessing the performance of Phyml 3.0. *Syst Biol* 2010;59:307–321.
 64. Huson DH, Bryant D. Application of phylogenetic networks in evolutionary studies. *Mol Biol Evol* 2006;23:254–267.
 65. Didelot X, Wilson DJ. ClonalframeML: Efficient inference of recombination in whole bacterial genomes. *PLoS Comp Biol* 2015;11:e1004041.
 66. Wheeler TJ, Eddy SR. NHMMER: DNA homology search with profile hmms. *Bioinformatics* 2013;29:2487–2489.
 67. Sullivan JT, Brown SD, Ronson CW. The NifA-RpoN regulon of *Mesorhizobium loti* strain R7A and its symbiotic activation by a novel LacI/GalR-family regulator. *PLoS One* 2013;8:e53762.
 68. Domazet-Lošo M, Haubold B. Alignment-free detection of local similarity among viral and bacterial genomes. *Bioinformatics* 2011;27:1466–1472.
 69. Shannon P, Markiel A, Ozier O, Baliga NS, Wang JT, et al. Cytoscape: A software environment for integrated models of biomolecular interaction networks. *Genome Res* 2003;13:2498–2504.
 70. Paradis E, Schliep K. Ape 5.0: An environment for modern phylogenetics and evolutionary analyses in R. *Bioinformatics* 2019;35:526–528.
 71. Huerta-Cepas J, Szklarczyk D, Heller D, Hernández-Plaza A, Forslund SK, et al. EggNOG 5.0: A hierarchical, functionally and phylogenetically annotated orthology resource based on 5090 organisms and 2502 viruses. *Nucleic Acids Res* 2019;47:D309–D314.
 72. Brynildsrud O, Bohlin J, Scheffer L, Eldholm V. Rapid scoring of genes in microbial pan-genome-wide association studies with scoary. *Genome Biol* 2016;17:238.
 73. van Heel AJ, de Jong A, Song C, Viel JH, Kok J, et al. BAGEL4: A user-friendly web server to thoroughly mine ribps and bacteriocins. *Nucleic Acids Res* 2018;46:W278–W281.
 74. Biswas A, Staals RHJ, Morales SE, Fineran PC, Brown CM. CRISPRDetect: A flexible algorithm to define CRISPR arrays. *BMC Genomics* 2016;17:356.
 75. Bekuma AA, Terpolilli JJ, Tiwari RP, O'Hara G, Howieson J, et al. *Biserrula pelecinus* L. is a promising forage legume for the central Ethiopian highlands. *Grass Forage Sci* 2021;00:1–11.

76. Garcillán-Barcia MP, Francia MV, de la Cruz F. The diversity of conjugative relaxases and its application in plasmid classification. *FEMS Microbiol Rev* 2009;33:657–687.
77. Li PL, Hwang I, Miyagi H, True H, Farrand SK. Essential components of the *ti* plasmid TRB system, a type IV macromolecular transporter. *J Bacteriol* 1999;181:5033–5041.
78. Li PL, Everhart DM, Farrand SK. Genetic and sequence analysis of the *ptic58 Trb* locus, encoding a mating-pair formation system related to members of the type IV secretion family. *J Bacteriol* 1998;180:6164–6172.
79. Cho H, Winans SC. TraA, TraC and TraD autorepress two divergent quorum-regulated promoters near the transfer origin of the Ti plasmid of *Agrobacterium tumefaciens*. *Mol Microbiol* 2007;63:1769–1782.
80. Carlton TM, Sullivan JT, Stuart GS, Hutt K, Lamont IL, et al. Ferrichrome utilization in a mesorhizobial population: Microevolution of a three-locus system. *Environ Microbiol* 2007;9:2923–2932.
81. Haase J, Kalkum M, Lanka E. Trbk, a small cytoplasmic membrane lipoprotein, functions in entry exclusion of the INCP alpha plasmid *rp4*. *J Bacteriol* 1996;178:6720–6729.
82. Bourdès A, Rudder S, East AK, Poole PS. Mining the *Sinorhizobium meliloti* transportome to develop fret biosensors for sugars, dicarboxylates and cyclic polyols. *PLoS One* 2012;7:e43578.
83. Marchetti M, Capela D, Poincloux R, Benmeradi N, Auriac M-C, et al. Queuosine biosynthesis is required for *Sinorhizobium meliloti*-induced cytoskeletal modifications on HeLa cells and symbiosis with *Medicago truncatula*. *PLoS One* 2013;8:e56043.
84. Ronson CW, Lyttleton P, Robertson JG. C(4)-dicarboxylate transport mutants of *Rhizobium trifolii* form ineffective nodules on *Trifolium repens*. *Proc Natl Acad Sci U S A* 1981;78:4284–4288.
85. Boesten B, Batut J, Boistard P. DctBD-dependent and -independent expression of the *Sinorhizobium (Rhizobium) meliloti* C4-dicarboxylate transport gene (*dctA*) during symbiosis. *MPMI* 1998;11:878–886.
86. Zehner S, Schober G, Wenzel M, Lang K, Göttfert M. Expression of the Bradyrhizobium japonicum type III secretion system in legume nodules and analysis of the associated TTS box promoter. *Mol Plant Microbe Interact* 2008;21:1087–1093.
87. Bendtsen JD, Kierner L, Fausbøll A, Brunak S. Non-classical protein secretion in bacteria. *BMC Microbiol* 2005;5:1–13.
88. Sugawara M, Takahashi S, Umehara Y, Iwano H, Tsurumaru H, et al. Variation in bradyrhizobial NOPP effector determines symbiotic incompatibility with Rj2-soybeans via effector-triggered immunity. *Nat Commun* 2018;9:1–12.
89. Cianciotto NP, White RC. Expanding role of type II secretion in bacterial pathogenesis and beyond. *Infect Immun* 2017;85.
90. Burrus V, Waldor MK. Formation of SXT Tandem arrays and SXT-R391 hybrids. *J Bacteriol* 2004;186:2636–2645.
91. Wozniak RA, Fouts DE, Spagnoletti M, Colombo MM, Ceccarelli D, et al. Comparative ICE genomics: Insights into the evolution of the *sxt/r391* family of ices. *PLoS Genet* 2009;5:12.
92. Spagnoletti M, Ceccarelli D, Rieux A, Fondi M, Taviani E, et al. Acquisition and evolution of SXT-R391 integrative conjugative elements in the seventh-pandemic *Vibrio cholerae* lineage. *mBio* 2AD;5:e01356-01314.
93. Bryant D, Moulton V. Neighbor-net: An agglomerative method for the construction of phylogenetic networks. *Mol Biol Evol* 2004;21:255–265.
94. Bruen TC, Philippe H, Bryant D. A simple and robust statistical test for detecting the presence of recombination. *Genetics* 2006;172:2665–2681.
95. Kuykendall LD, Shao JY, Hartung JS. “Ca. *Liberibacter asiaticus*” proteins orthologous with pSymA-encoded proteins of *Sinorhizobium meliloti*: hypothetical roles in plant host interaction. *PLoS One* 2012;7:e38725.
96. Makarova KS, Wolf YI, Alkhnbashi OS, Costa F, Shah SA, et al. An updated evolutionary classification of CRISPR-Cas systems. *Nat Rev Microbiol* 2015;13:722–736.
97. Koonin EV, Makarova KS, Zhang F. Diversity, classification and evolution of CRISPR-Cas systems. *Curr Opin Microbiol* 2017;37:67–78.
98. Biswas A, Gagnon JN, Brouns SJJ, Fineran PC, Brown CM. CRISPRTarget: Bioinformatic prediction and analysis of CRRNA targets. *RNA Biol* 2013;10:817–827.
99. Li X, Wang H, Tong W, Feng L, Wang L, et al. Exploring the evolutionary dynamics of *Rhizobium* plasmids through bipartite network analysis. *Environ Microbiol* 2020;22:934–951.
100. Cury J, Oliveira PH, de la Cruz F, Rocha EPC. Host range and genetic plasticity explain the coexistence of integrative and extrachromosomal mobile genetic elements. *Mol Biol Evol* 2018;35:2230–2239.
101. Thomas CM, Nielsen KM. Mechanisms of, and barriers to, horizontal gene transfer between bacteria. *Nat Rev Microbiol* 2005;3:711–721.

Five reasons to publish your next article with a Microbiology Society journal

1. The Microbiology Society is a not-for-profit organization.
2. We offer fast and rigorous peer review – average time to first decision is 4–6 weeks.
3. Our journals have a global readership with subscriptions held in research institutions around the world.
4. 80% of our authors rate our submission process as ‘excellent’ or ‘very good’.
5. Your article will be published on an interactive journal platform with advanced metrics.

Find out more and submit your article at microbiologyresearch.org.